

Diffuse reflection high-energy electron diffraction

U. Korte and G. Meyer-Ehmsen

Fachbereich Physik, Universität Osnabrück, 49069 Osnabrück, Germany

(Received 17 December 1992)

A numerically manageable formalism for the dynamical calculation of diffuse reflection high-energy electron diffraction (RHEED) is presented. The diffuse scattering arises from transitions between dynamically calculated scattering states in the periodic part of the scattering potential and the nonperiodic part is treated as a perturbation. For atoms placed on equivalent lattice sites relative to the periodic-potential part, the formalism allows us to treat disorder scattering by kinematical structure factors that have to be multiplied by dynamically calculated atomic-scattering amplitudes so that the statistics of the disorder can be treated independently of the dynamical calculations. It is shown that azimuthal reflection profiles (parallel to the shadow edge) can, in favorable cases, be interpreted kinematically whereas polar profiles (normal to the shadow edge) are strongly influenced dynamically. It is further demonstrated by model calculations for the diffuse RHEED from disordered adsorbate layers that the corresponding broad scattering distribution depends strongly on the position of the adsorbate relative to the substrate. This should enable the use of RHEED in the field of structure analysis of disordered adsorbate layers. Finally, our concept is applied to thermal diffuse scattering. We show that the main structures of a measured broad thermal-diffuse-scattering distribution from Pt(110) can be explained with the Einstein model, i.e., independent atomic oscillations.

I. INTRODUCTION

Reflection high-energy electron diffraction (RHEED) intensities from perfectly periodic surfaces can be calculated in a straightforward way. Since the interaction of the electrons with the solid is relatively strong, a dynamical diffraction theory, where multiple scattering is taken into account, has to be used. A number of such calculations by various methods have been presented; see, e.g., Refs. 1–7. Besides the wide application of RHEED in the study of molecular-beam epitaxy and thin-film growth techniques,^{8–10} it has also been used successfully in surface crystallography by comparisons between dynamical theory and experimental data.^{11–14} The accuracy is similar to the accuracy reached in low-energy electron diffraction (LEED). The compared intensity data are usually rocking curves of reflections, i.e., intensity of a reflection versus incident angle of the primary beam at fixed electron energy. The structure analysis is performed by fitting model parameters to the experimental data.

Diffuse scattering appears if momentum transfer is not restricted to the reciprocal vectors of the surface lattice. This is the case if the surface exhibits disorder or inelastic-scattering processes, e.g., thermal diffuse scattering (TDS), occur. So far, the interpretation of diffuse scattering in RHEED has been based mainly on the single scattering approach (kinematical theory). In LEED a (pseudo)kinematical theory has been successfully used in many cases in order to interpret diffuse scattering due to structural surface disorder. Equivalent approaches were applied in RHEED for the analysis

of step distributions.^{15–18} Principle features in RHEED arising from surface disorder are discussed in Ref. 19 also from a kinematical point of view.

However, a justification for the use of the kinematical approximation in diffuse RHEED has not been given so far. It is known from many publications^{20–22} that diffuse scattering in RHEED has in principle to be calculated with a dynamical theory (as is the case for scattering into the sharp reflections). Although this is generally accepted, an evaluation scheme for the analysis of diffuse RHEED, which is based on the dynamical theory and numerically manageable, has not been presented so far. There are several rigorous calculations where special situations are considered, e.g., diffraction from one single step²³ or from large supercells where the disorder is included in the cell.²⁴ The analysis of experimental diffraction data, however, would require the calculation of the scattering from many statistically varying configurations. This would lead to such an enormous computational effort that the interpretation by rigorous calculations seems to be hopeless.

In this paper we present a formalism which treats the dynamical diffuse scattering as a transition between states [two-dimensional (2D) Bloch waves] in the periodic part of the potential. The nonperiodic part is treated as a perturbation. Such a treatment is similar to the calculation of diffuse LEED (Ref. 25) and also extended x-ray-absorption fine-structure techniques.²⁶ Moreover, dynamical electron diffraction before the transition plays an important role for Auger excitation.^{27,28} An example where dynamical electron diffraction after the transition has to be taken into account is ultraviolet photoemission spectroscopy.^{29,30}

In our approach for RHEED the diffraction before and after the diffuse scattering event is described *fully dynamically*. This allows the calculation of Kikuchi lines, bands and envelopes by using appropriate interaction potentials for the diffuse scattering process. The approach leads further to an expression where scattering from atoms distributed statistically on equivalent lattice sites relative to the periodic potential part is given by means of *kinematical* calculated structure factors multiplied by *dynamically* calculated atomic-scattering amplitudes. In this way the problem of many configurations is overcome (as long as the nonperiodic part can be treated as a perturbation).

In a recent paper³¹ we outlined the calculation scheme for special cases in connection with the Pt(110)(1×2) \rightleftharpoons (1×1) order disorder transition. It was shown that diffraction effects from two-dimensional disorder and from steps which could not be explained kinematically were reproduced rather well.

Here we present the method in detail and from a more general point of view. At first we will derive the formalism in terms of the R -matrix method for RHEED calculations⁶ where the reflectivity of the surface is gained by direct integration of the reflectivity (R) matrix. We will use this scheme in its "smoothed" form, i.e., rapid oscillations of the wave field normal to the surface are removed in order to allow a numerically fast solution of the corresponding differential equations. The validity of the method will be checked by means of a simple example where the perturbational treatment is compared with a rigorous calculation.

Next we derive the concept of the kinematical structure factors and dynamical atomic-scattering amplitudes f_{dyn} . The similarity of $|f_{\text{dyn}}|^2$ with experimental Kikuchi patterns will be demonstrated. It will also be shown that in certain cases, namely if f_{dyn} remains constant within the region in reciprocal space where a reflection profile is to be investigated, a kinematical-like evaluation of experimental data is possible. In particular, azimuthal reflection profiles parallel to the shadow edge can in some cases be interpreted kinematically. Profiles normal to the shadow edge, which correspond to disorder along the incidence azimuth, are usually strongly influenced by dynamical scattering.

Furthermore, we will discuss the possibility of using diffuse RHEED as a tool for structural investigations of disordered adsorbate layers, similar to the case of "diffuse LEED."³² It turns out from model calculations that the scattering distribution induced by the adsorbate depends significantly on the position of the adsorbate relative to the substrate.

Finally, the paper contains a section on TDS. We compare a measured TDS distribution with a calculation based on a simple expression for the vibration-induced perturbation potential. The comparison reveals that the modulations of the observed broad scattering distribution are obviously influenced by dynamical scattering rather than by correlations between the vibrating atoms. This may be used to account for TDS in a simple way if it is superimposed to other diffuse scattering distributions to be investigated, e.g., the scattering from disordered adsorbate layers, as mentioned above.

II. CALCULATION OF DIFFUSE RHEED

A. Computational method

The electron wave field under RHEED conditions is theoretically properly described in terms of a (two-dimensional) plane-wave representation of the Schrödinger equation

$$\mathbf{y}''(z) = [(i\mathbf{K})^2 + \mathbf{V}(z)]\mathbf{y}(z) \quad (1)$$

where z is the coordinate normal to the surface. The diagonal matrix \mathbf{K} contains the z components of the wave vectors corresponding to the scattering vectors \mathbf{s} parallel to the surface (see below). Vector \mathbf{y} contains the 2D Fourier components $y_{\mathbf{s}}(z)$ of the wave function

$$\psi(\mathbf{r}) = \exp(i\mathbf{k}_{0t} \cdot \mathbf{r}_t) \sum_{\mathbf{s}} y_{\mathbf{s}}(z) \exp(i\mathbf{s} \cdot \mathbf{r}_t). \quad (2)$$

\mathbf{k}_{0t} and \mathbf{r}_t are the tangential components of the incident wave vector and the real-space coordinate, respectively. \mathbf{s} denotes the (2D) vectors in reciprocal space which are in the case of a perfect periodic surface the reciprocal surface lattice vectors \mathbf{g} . The "strength" of dynamical coupling between waves being indexed with \mathbf{s} and \mathbf{s}' , respectively, is given by the Fourier coefficients $V_{\mathbf{s}-\mathbf{s}'}(z)$ [matrix $\mathbf{V}(z)$ in Eq. (1)] of the scattering potential $V(\mathbf{r})$.

In our formulation we use the R -matrix method⁶ in order to solve Eq. (1). With the definition (see Ref. 3)

$$\mathbf{y}(z) = \exp(i\mathbf{K}z)\mathbf{f}(z) + \exp(-i\mathbf{K}z)\mathbf{b}(z) \quad (3)$$

the reflectivity matrix \mathbf{R} relates the forward traveling waves $\exp(i\mathbf{K}z)\mathbf{f}(z)$ to the backward traveling ones $\exp(-i\mathbf{K}z)\mathbf{b}(z)$:

$$\exp(-i\mathbf{K}z)\mathbf{b}(z) = \mathbf{R}(z)\exp(i\mathbf{K}z)\mathbf{f}(z). \quad (4)$$

Furthermore, the subsidiary condition

$$\exp(i\mathbf{K}z)\mathbf{f}'(z) + \exp(-i\mathbf{K}z)\mathbf{b}'(z) = 0 \quad (5)$$

is introduced. Using Eqs. (3) and (5), the second-order system (1) is transformed into the nonlinear first-order system

$$\mathbf{R}'(z) = -i\mathbf{K}\mathbf{R}(z) - \mathbf{R}(z)i\mathbf{K} - [\mathbf{1} + \mathbf{R}(z)](2i\mathbf{K})^{-1}\mathbf{V}(z)[\mathbf{1} + \mathbf{R}(z)]. \quad (6)$$

The reflectivity matrix \mathbf{R} contains rapidly oscillating terms $\propto \exp(-2ik_z)$, which can be eliminated if the smoothed reflectivity matrix

$$\mathbf{M}(z) = \exp(i\mathbf{W}z)\mathbf{R}(z)\exp(i\mathbf{W}z), \quad (7)$$

with $\mathbf{W} = \text{Re}(\mathbf{K})$, is integrated instead of \mathbf{R} . Inserting (7) into (6) reveals the smoothed differential equation system

$$\begin{aligned} \mathbf{M}' &= \mathbf{L}\mathbf{M} + \mathbf{M}\mathbf{L} \\ &\quad - [\exp(2i\mathbf{W}z) + \mathbf{M}]\mathbf{P}[\exp(2i\mathbf{W}z) + \mathbf{M}], \\ \mathbf{P} &= \exp(-i\mathbf{W}z)[2i\mathbf{K}]^{-1}\mathbf{V}\exp(-i\mathbf{W}z), \end{aligned} \quad (8)$$

where $\mathbf{L} = \text{Im}(\mathbf{K})$. The following discussion refers to this

representation.

A nonperiodic surface has a continuous Fourier spectrum so that the dimension of the system (8) gets infinite (even if only a finite region of reciprocal space is taken into account). A numerically reasonable discretization of the spectrum would lead to enormously large computing times, in particular if one keeps in mind that in many cases the scattering of a large number of configurations has to be computed in order to take the statistics of the perturbation into account. Such calculations were performed by Knibb.²⁴

We decompose the scattering potential $V(\mathbf{r})$ of each atomic layer into a laterally periodic (p) and a non-periodic diffuse (d) part:

$$V = V_p + V_d. \quad (9)$$

V_p contains only Fourier coefficients at the reciprocal surface lattice points \mathbf{g} and defines the mean periodic potential whereas the diffuse part V_d consists of all components at $\mathbf{s} \neq \mathbf{g}$. Provided that the Fourier coefficients of the diffuse part V_d are sufficiently small, mainly the periodic part V_p is responsible for the dynamical beam coupling. Then the coupling between *diffuse* waves cannot be neglected if a vector \mathbf{g} of the reciprocal lattice corresponding to V_p is transferred. Diffuse waves, being coupled again to diffuse waves $\mathbf{s} \neq \mathbf{g}$, have only second-order influence on the potential matrix \mathbf{P} . Their influence can be taken phenomenologically into account as a part of the absorption potential which is usually treated as a fit parameter. The diffuse scattering into a direction which corresponds to a scattering vector

$$\mathbf{s}_0 = \mathbf{g}_0 + \mathbf{u} \quad (10)$$

(\mathbf{u} lying in the first surface Brillouin zone) is therefore dominated by a set of reciprocal rods which includes

$$(i) \text{ the reciprocal lattice vectors } \mathbf{g} \quad (11)$$

and

$$(ii) \text{ all diffuse vectors with } \mathbf{s} = \mathbf{g} + \mathbf{u}. \quad (12)$$

These rods should be included in the calculation. An illustration is shown in Fig. 1. It is clear that for each \mathbf{s}_0 , a different set of rods according to Eq. (12) has to be used.

Now we will transform Eq. (8) into a proper form which allows the direct calculation of the diffuse scattering in

first order of the perturbation. For this purpose, the relevant matrices of the system (8) are decomposed into submatrices corresponding to the two kind of rods, namely \mathbf{g} and $\mathbf{g} + \mathbf{u}$:

$$\mathbf{L} = \begin{pmatrix} \mathbf{L}_p & \mathbf{0} \\ \mathbf{0} & \mathbf{L}_d \end{pmatrix}, \quad \mathbf{W} = \begin{pmatrix} \mathbf{W}_p & \mathbf{0} \\ \mathbf{0} & \mathbf{W}_d \end{pmatrix}, \quad (13)$$

$$\mathbf{M} = \begin{pmatrix} \mathbf{M}_{pp} & \mathbf{M}_{pd} \\ \mathbf{M}_{dp} & \mathbf{M}_{dd} \end{pmatrix}, \quad \mathbf{P} = \begin{pmatrix} \mathbf{P}_{pp} & \mathbf{P}_{pd} \\ \mathbf{P}_{dp} & \mathbf{P}_{dd} \end{pmatrix}.$$

The index p stands for the reciprocal lattice vectors \mathbf{g} of the periodic potential V_p ; the index d denotes the set of diffuse scattering vectors $\mathbf{s} \neq \mathbf{g}$ according to Eq. (12). We note that dd means a *strong* coupling (via V_p) between the diffuse scattering vectors separated by reciprocal lattice vectors \mathbf{g} . Now the matrices in their decomposed form (13) are inserted into the fundamental system (8). On performing the necessary matrix multiplications, all contributions are neglected which contain the weak couplings dp and pd in second and higher order. The result is

$$\mathbf{M}'_{pp} = \mathbf{L}_p \mathbf{M}_{pp} + \mathbf{M}_{pp} \mathbf{L}_p - [\exp(2i\mathbf{W}_p z) + \mathbf{M}_{pp}] \mathbf{P}_{pp} [\exp(2i\mathbf{W}_p z) + \mathbf{M}_{pp}],$$

$$\mathbf{M}'_{dd} = \mathbf{L}_d \mathbf{M}_{dd} + \mathbf{M}_{dd} \mathbf{L}_d - [\exp(2i\mathbf{W}_d z) + \mathbf{M}_{dd}] \mathbf{P}_{dd} [\exp(2i\mathbf{W}_d z) + \mathbf{M}_{dd}],$$

$$\mathbf{M}'_{dp} = \mathbf{L}_d \mathbf{M}_{dp} + \mathbf{M}_{dp} \mathbf{L}_p - \mathbf{M}_{dp} \mathbf{P}_{pp} [\exp(2i\mathbf{W}_p z) + \mathbf{M}_{pp}] - [\exp(2i\mathbf{W}_d z) + \mathbf{M}_{dd}] \mathbf{P}_{dd} \mathbf{M}_{dp} - [\exp(2i\mathbf{W}_d z) + \mathbf{M}_{dd}] \mathbf{P}_{dp} [\exp(2i\mathbf{W}_p z) + \mathbf{M}_{pp}]. \quad (14)$$

In the equation for \mathbf{M}_{dp} the first three terms describe fully dynamically the propagation of the diffusely scattered waves in the periodic part of the potential. Therefore, these terms are always responsible for the appearance of Kikuchi-like patterns with general shapes (but not intensities) being mainly independent from the exact type of the perturbation.

The last term in \mathbf{M}_{dp} contains the first-order diffuse scattering processes between fully dynamically calculated scattering states (2D Bloch waves) in the periodic potential.

The (smoothed) reflected amplitudes are obtained by integrating (e.g., using the standard Runge-Kutta-Merson method) the system (14) from the crystal slab rear side ($z = t$) to the surface ($z = 0$) with the starting condition $\mathbf{M}(z = t) = 0$ as described in Ref. 6. After the system has been solved, the nonsmoothed reflectivities \mathbf{R} are obtained by the transformation

$$\mathbf{R}_{pp} = \exp(-i\mathbf{W}_p z) \mathbf{M}_{pp} \exp(-i\mathbf{W}_p z), \quad (15)$$

$$\mathbf{R}_{dp} = \exp(-i\mathbf{W}_d z) \mathbf{M}_{dp} \exp(-i\mathbf{W}_p z).$$

The column R_{d0} contains the diffuse amplitudes reflected into the vacuum.

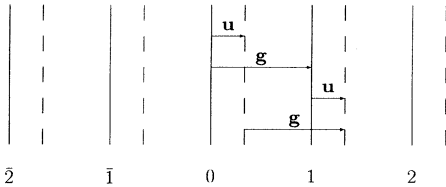


FIG. 1. Set of lattice rods used to calculate the diffuse scattering into directions corresponding to $\mathbf{g} + \mathbf{u}$. \mathbf{g} denotes a reciprocal rod of the periodic part of the scattering potential.

The equations for \mathbf{M}_{pp} and \mathbf{M}_{dd} in the system (14) correspond to (two-dimensional) Bloch states in the periodic potential and the diffuse scattering \mathbf{M}_{dp} is caused by transitions between these states due to the nonperiodic potential. Dudarev, Peng, and Ryzanov³³ developed a similar formalism especially for thermal diffuse scattering as transitions between scattering states in the periodic potential. Our approach allows a comparably simple numerical evaluation for many beams because only a system of first-order differential equations has to be solved. In particular, we would like to stress that the calculational effort per angle is *only three times* as much as the effort for a conventional calculation for a perfect periodic structure. The reason for this quite low effort is that the system (14) to be solved consists of three subsystems, each of which with about the same number of necessary matrix multiplications as in the case of a conventional calculation.

In the following we will discuss the validity as well as the application of the formalism to surface disorder, scattering from adsorbates, and thermal diffuse scattering. The model calculations and comparisons with experimental data to be presented concern mainly the Pt(110)(1×2) surface (missing row^{34–36}) and its $(1 \times 2) \rightleftharpoons (1 \times 1)$ order disorder transition at elevated crystal temperatures. The periodic part of the potential needed for the calculation of the diffuse scattering was taken from the RHEED structure analysis published before.¹⁴ The incidence azimuth was $[1\bar{1}0]$ at 19 keV electron energy. Twenty-five reciprocal lattice rods in the zeroth Laue zone were taken into account for the calculation of the dynamical scattering within the periodic-potential part. It has been checked that additional rods do not change the results significantly.

In one case (Sec. III B) also data for Pt(111) are presented. Here, a five-rod calculation (19 keV) in the $[11\bar{2}]$ azimuth was used where the periodic part of the potential was ascribed to a nonrelaxed bulk-terminated structure.

B. Validity of the method

It is difficult to estimate the accuracy of the calculation scheme presented. Generally, it will work as long as in reciprocal space the nonperiodic part V_{dp} is sufficiently small. The range of validity of the approximation can only be checked by a comparison with experimental data or exact calculations. The latter is very difficult because the application of the conventional computing methods for dynamical RHEED would require a discretization of the *continuous* function V_{dp} . Furthermore, the problem would arise that the scattering from a very large number of statistical configurations has in principle to be considered.

In order to get an idea whether the strength of V_{dp} is very critical, we have calculated rocking curves for the Pt(110)(1×2) reconstructed surface (electron energy 19 keV, incident azimuth $1\bar{1}0$). The (1×2) reconstruction is due to the missing-row model: each second close-packed atomic chain along $[1\bar{1}0]$ in the first layer is missing. We have performed exact calculations and calculations using our approximation presented where the

twofold periodicity was treated as the perturbation V_{dp} . In this sense, the half-order reflections due to the (1×2) reconstruction are regarded as the diffuse scattering. The strength of V_{dp} in the exact calculation was altered by multiplying the half-order Fourier coefficients with a factor ψ . The factor ψ represents the ratio of the diffuse and periodic potential part in the first layer. We note that ψ can also be regarded as a long-range order parameter of the twofold periodicity.¹⁴ In the case of the approximative calculation, the structure of the curves does not depend on ψ because the diffuse scattering amplitude is linear with regard to V_{dp} (see also Sec. III). Also the rocking curves belonging to whole-order reflections do not depend on ψ in the approximative case because the dynamical coupling by half-order Fourier coefficients is neglected.

Figure 2 shows a quantified comparison between exact and perturbation calculations, dependent on the factor ψ . The degree of agreement is expressed in terms of the metric distance D_{rms} between both kind of curves. D_{rms} denotes the (normalized) root-mean-square deviation as introduced in Ref. 14. $D_{\text{rms}} = 0$ means perfect agreement whereas $D_{\text{rms}} = 1$ corresponds to no correlation

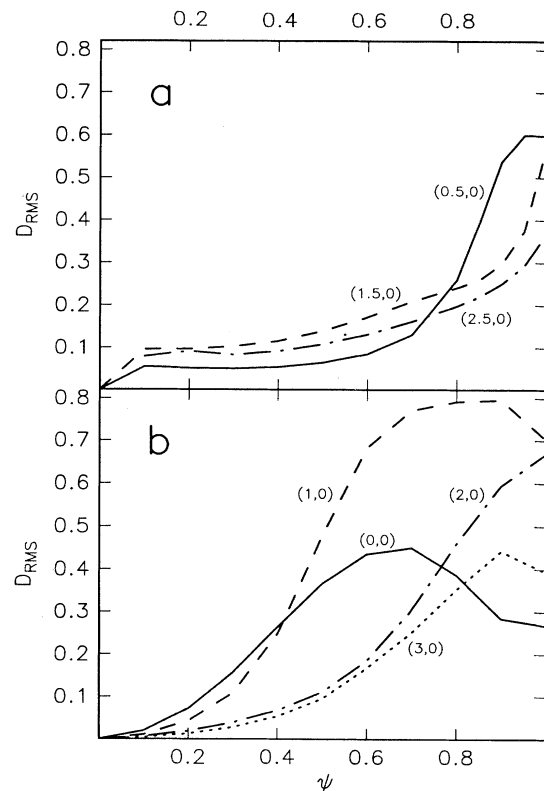


FIG. 2. Root-mean-square distance between exact and perturbation calculations for rocking curves from the Pt(110)(1×2) surface (19 keV, azimuth $[1\bar{1}0]$), dependent on the strength ψ of the perturbation (half-order Fourier coefficients). ψ can be regarded as the ratio between the diffuse and periodic parts of the potential in the first layer. (a) Comparison for the half-order (“diffuse”) reflections; (b) comparison for the integral-order reflections.

between the compared curves. Figure 2(a) shows the behavior for the half-order (diffuse) reflections (0.5,0), (1.5,0), and (2.5,0) whereas in Fig. 2(b) the situation for the whole-order reflections (0,0), (1,0), (2,0), and (3,0) is demonstrated. The agreement between exact and perturbation calculations for the diffuse intensity is aston-

ishingly good, even up to the ratio $\psi \approx 0.6$ where the worst metric distance is about $D_{\text{rms}} = 0.2$ for the (1.5,0) reflection. Up to $\psi \approx 0.4$ the distance is better than 0.1. One has to keep in mind that the best agreement between RHEED theory and experimental data so far achieved is of the order $D_{\text{rms}} = 0.15$.¹⁴

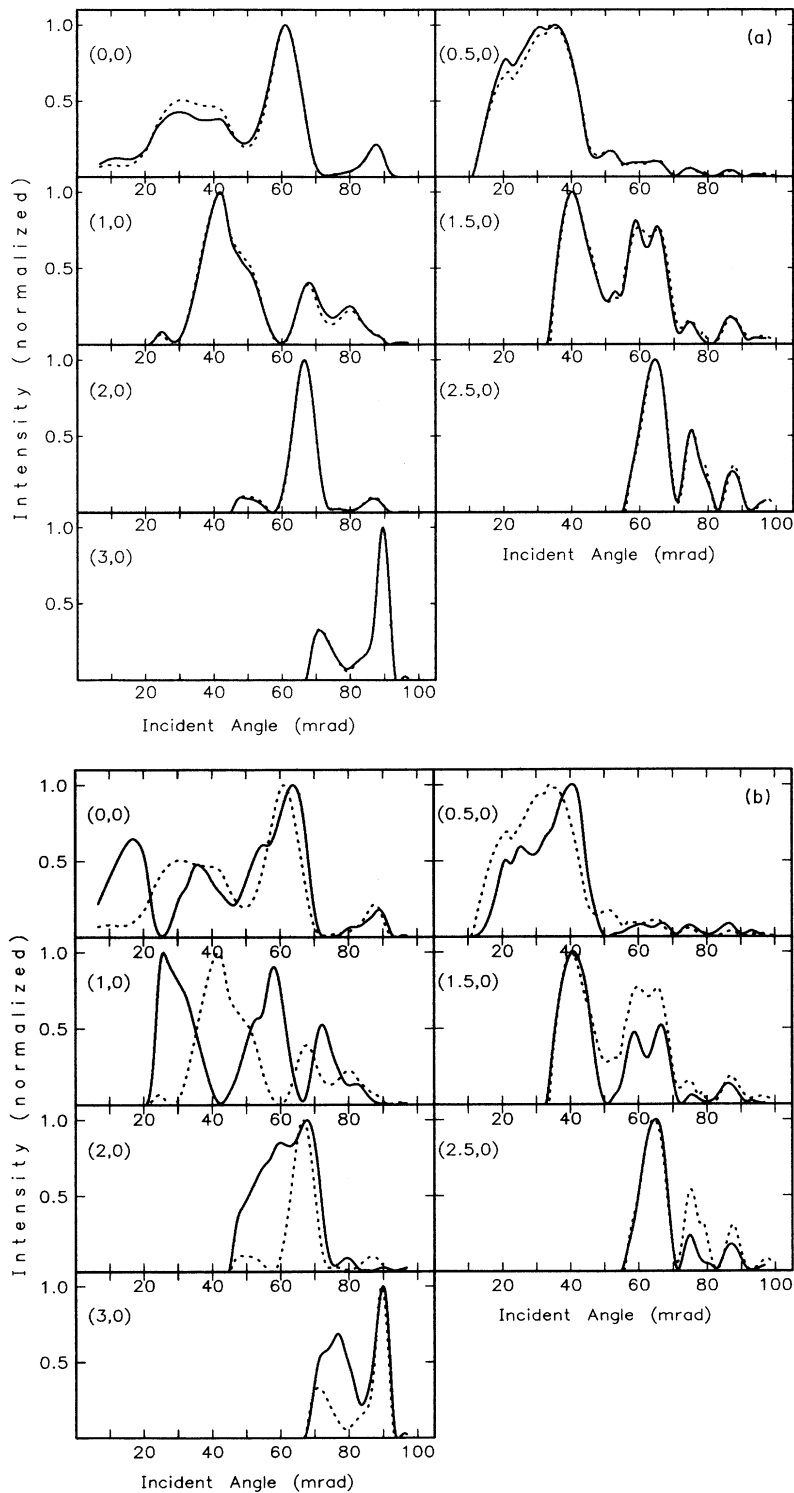


FIG. 3. Rocking curves from exact and perturbation calculations compared for (a) $\psi = 0.2$ and (b) $\psi = 0.8$ (see also Fig. 2). The excellent agreement between both calculations in (a) is evident.

For the integral-order reflection the situation is a bit worse. Here, the approximative calculation works up to a ratio of about $\psi = 0.3$. The reason for this minor agreement can be quite easily understood: The approximation neglects all dynamical beam couplings via half-order lateral momentum transfer. In the case of the fractional beams, the first-order momentum transfer (integral \rightarrow half) is included. Second-order fractional terms do not contribute to the half-order intensity because they always lead to momentum transfer into the integral beams. Hence the first neglected contribution in the case of the fractional beams is of *third* order while for the integral beams, the first neglected contribution is already of *second* order.

Figure 3 shows exemplary sets of rocking curves for two cases: Fig. 3(a), $\psi = 0.2$, where the approximation works well and Fig. 3(b), $\psi = 0.8$, where the perturbation calculation is not allowed. The very good agreement between the approximation and the exact calculation for the smaller ψ is evident.

III. SCATTERING FROM DISORDERED SURFACES

A. The pseudokinematical scattering formula

Equation (14) allows further simplifications. Using the starting condition $\mathbf{M}(t) = \mathbf{0}$ at the crystal rear side ($z = t$), one can easily show that the solutions for the submatrix \mathbf{M}_{dp} are linear functionals with regard to the perturbation \mathbf{P}_{dp} ; i.e.,

$$\begin{aligned} \mathbf{M}_{dp}(\mathbf{P}_{1,dp} + \mathbf{P}_{2,dp}) &= \mathbf{M}_{dp}(\mathbf{P}_{1,dp}) + \mathbf{M}_{dp}(\mathbf{P}_{2,dp}), \\ \mathbf{M}_{dp}(\alpha\mathbf{P}_{1,dp}) &= \alpha\mathbf{M}_{dp}(\mathbf{P}_{1,dp}) \end{aligned} \quad (16)$$

in case of two perturbations $\mathbf{P}_{1,dp}$ and $\mathbf{P}_{2,dp}$. This allows us to calculate the scattering of different perturbations separately followed by a superposition of the single contributions.

A very important aspect of the linearity appears in the case of diffuse scattering from an ensemble of atoms on equivalent sites relative to the periodic part of the potential. Equivalent sites are separated by two-dimensional translations \mathbf{T} , which are compatible with the reciprocal lattice vectors \mathbf{g} . Let $v_1(\mathbf{r})$ and $v_2(\mathbf{r}) = v_1(\mathbf{r} + \mathbf{T})$ be the potentials of such two atoms. The corresponding elements of the potential matrices $v_{1,\mathbf{sg}}(z)$ and $v_{2,\mathbf{sg}}(z)$ [$\mathbf{s} = \mathbf{h} + \mathbf{u}$ according to Eq. (12)] differ only by the phase factor

$$\mathbf{v}_2 = \exp(i\mathbf{u}\mathbf{T})\mathbf{v}_1. \quad (17)$$

Hence, if we call the dynamical calculated scattering amplitude (reflectivity R_{do}) for a single atom f_{dyn} and use the linearity (16), the scattering amplitude F of the whole ensemble is given by the superposition

$$F = f_{dyn}(\mathbf{s}) \sum_n \exp(i\mathbf{r}_n \cdot \mathbf{u}). \quad (18)$$

\mathbf{r}_n denotes the (lateral) coordinate of the atom n . This result is identical to the kinematical scattering formula,

except that the kinematical atomic-scattering amplitude is replaced by the dynamical scattering amplitude f_{dyn} . Once f_{dyn} is known, all statistical concepts of the kinematical theory can be applied. In particular, the direct dynamical calculation of scattering from many configurations, which would be enormously time consuming, is not necessary.

If atoms with different types of sites relative to the periodic-potential part play a role, Eq. (18) has to be extended to

$$F = \sum_i f_{dyn,i} \sum_n \exp(i\mathbf{r}_{n,i} \cdot \mathbf{u}). \quad (19)$$

Here, the index i labels the different types of sites. For fixed i , all $\mathbf{r}_{n,i}$ have to be separated by translations compatible with the reciprocal surface lattice vectors, respectively. In this case of various $f_{dyn,i}$, the evaluation of measured intensities can, for instance, be performed following the kinematical scheme for LEED published by Jagodzinski, Moritz, and Wolf.³⁷

We further note that the dynamical scattering amplitude f_{dyn} has a different meaning than the multiple-scattering amplitude in the case of LEED.^{37,38} Because of the low energy, the multiple-scattering amplitude in LEED usually refers to a surface area of comparably small extension so that for atoms with different local surroundings different dynamical amplitudes have to be calculated. In RHEED, however, the position relative to the mean periodic potential determines the influence of the multiple scattering.

B. Dynamical and kinematical RHEED

It is obvious that a completely kinematical evaluation of diffuse RHEED is possible as long as the absolute amount $|f_{dyn}(\mathbf{s})|^2$ of the dynamical scattering amplitude remains constant within the analyzed region in reciprocal space [see Eq. (18)]. In the following we will check whether this can be fulfilled.

In Fig. 4 we show the calculated intensity distribution of $|f_{dyn}|^2$ for an atom in the top layer of the Pt(110)(1×2) surface. The perturbation atom is situated within the first layer on a lattice site between the atomic rows, i.e., out of phase relative to the (1×2) periodicity.

Diffuse RHEED usually appears as elongated streaks (normal to the shadow edge) around sharp reflection spots. Figure 4 shows that the angular scale of the modulations of $|f_{dyn}|^2$ along the azimuthal exit direction (parallel to the surface and perpendicular to the incidence azimuth) is of the order of the extension of the (surface) Brillouin zone in that direction. In most cases, however, the extension of reflection profiles in reciprocal space is much smaller than the Brillouin zone. Thus the azimuthal reflection profiles across the streaks, which reflect the surface disorder *across* the incident azimuth, can indeed be interpreted kinematically in many cases.

In the case of the polar exit direction, the situation is more complicated. The corresponding reflection profiles along the streaks reflect the disorder *along* the incident azimuth—the direction where RHEED has its high spa-

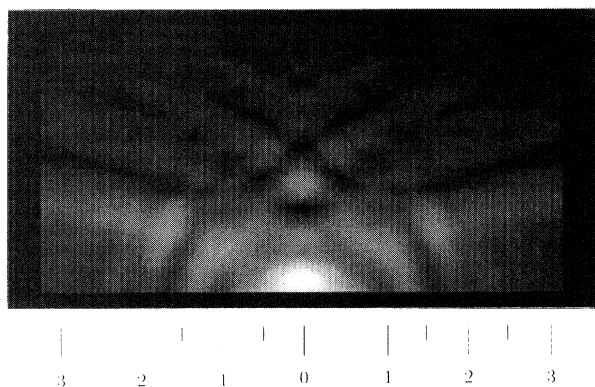


FIG. 4. Calculated scattering distribution from a perturbation atom in the top layer of the Pt(110)(1 × 2) surface. The atom is situated within the first layer between the atomic rows, i.e., out of phase relative to the (1 × 2) periodicity. Energy, 19 keV; incident glancing angle, 95 mrad; angular area, 150 × 90 mrad. The lower margin corresponds to the polar exit angle 12 mrad; the center of the picture corresponds to the exit azimuth [1 $\bar{1}$ 0]. Bright regions mean high intensity. The resolution is 1 × 1 mrad.

tial resolution. Because of the glancing incidence geometry, the polar angular extension of the Brillouin zone in the diffraction pattern is very large (in Fig. 4, larger than the plotted picture) so that the angular scale of modulations of $|f_{\text{dyn}}|^2$ along the polar direction is small compared to the size of the Brillouin zone. Consequently, polar reflection profiles have to be interpreted dynamically.

It is indeed a commonly observed phenomenon that modulations of RHEED reflection profiles appear along the streaks but not across them; e.g., see Refs. 21 and 22.

Figure 5 demonstrates the influence of the dynamical scattering in the case of a polar profile [Pt(110)(1 × 2), scan through the (0.5, 0) reflection for the [1 $\bar{1}$ 0] incident azimuth]. The diffuse scattering around half-order reflections is due to antiphase domains relative to (1 × 2). It indicates the beginning of the phase transition into a disordered (1 × 1) structure.^{39,14,40} In the lower panel, the measured profile (solid line) is shown. It exhibits modulations which kinematically cannot be understood. The upper panel shows a purely kinematical profile in case of a Gaussian pair correlation, the width of which has been fitted to the experiment (see also Ref. 31). The middle panel shows the dynamical atomic form factor $|f_{\text{dyn}}|^2$ calculated with our theory. Note the significant modulation of this factor which would, in the kinematical case, practically be a constant. The dashed line in the lower panel illustrates the Gaussian profile multiplied by $|f_{\text{dyn}}|^2$, which reveals an excellent agreement with the observed profile.

Further measured and calculated polar profiles (for different reflections and various incident angles) concerning the Pt(110)(1 × 2) \rightleftharpoons (1 × 1) phase transition have recently been published in Ref. 31 where more details for this special system can be found.

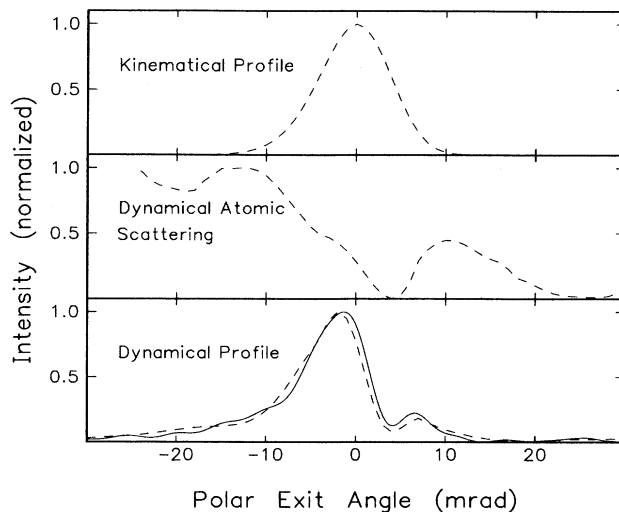


FIG. 5. Influence of the dynamical scattering on a polar reflection profile for the (0.5, 0) reflection from Pt(110)(1 × 2); see text. Azimuth [1 $\bar{1}$ 0], 19 keV, incident glancing angle 48 mrad. The origin of the angular scale corresponds to the Laue circle. Upper panel, pure kinematical profile corresponding to the structure factor; middle panel, dynamical scattering intensity due to one atom; lower panel, dynamical calculated profile (dashed line) and corresponding experimentally measured curve (solid line). The dynamical profile is the product of the kinematical profile and the dynamical scattering intensity.

It is clear that the amount of structure or modulations in the dynamical profile depends on the (kinematical) broadening of the reflection under consideration. With increasing broadening of the profile, the influence of the strongly modulated dynamical form factor f_{dyn} on the profile shape becomes more and more important. Following this line, the agreement of the theory with the experiment might get worse with increasing profile width because the dynamical form factor is essentially affected by the periodic part of the scattering potential of the near surface layers. Although this potential part can in principle be extracted from rocking curves by dynamical evaluation quite well, it is certainly not known perfectly. Consequently, if quantitative data concerning structural disorder are to be determined experimentally, diffraction conditions or regions in reciprocal space should be chosen where modulations of f_{dyn} are minimized as far as possible. Examples for profiles with strong and weak modulations can also be found in Ref. 31.

As already mentioned above, the possibility of a kinematical interpretation of *azimuthal* profiles depends strongly on the strength of the angular modulations of the dynamical scattering factor f_{dyn} . A more critical situation with stronger modulations than in the case of Fig. 4 is demonstrated in Fig. 6(a). Here, the calculated intensity distribution of $|f_{\text{dyn}}|^2$ is shown for the Pt(111) surface in the [11 $\bar{2}$] incident azimuth. The appearance of comparably rapid modulations is evident. Furthermore, we note that these features are correlated with Kikuchi

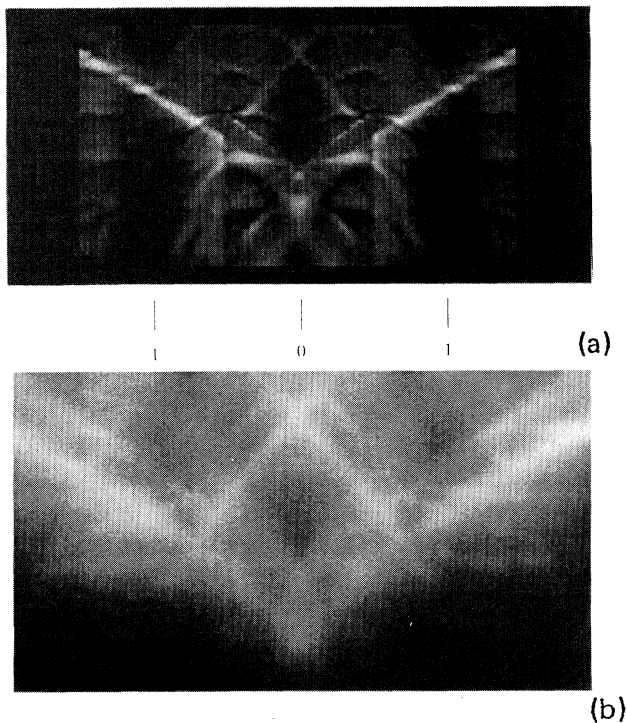


FIG. 6. (a) Calculated scattering distribution from a perturbation atom in the top layer of the Pt(111) surface. The atom is situated on a lattice site. Energy, 19 keV; incident glancing angle, 120 mrad; angular area 190×110 mrad. The lower margin corresponds to the polar exit angle 20 mrad; the center of the picture corresponds to the exit azimuth $[11\bar{2}]$. Bright regions mean high intensity. The resolution is 1×1 mrad. (b) Experimental diffuse scattering distribution for the same angular region. Note the correlation between the Kikuchi patterns in (b) and the features in (a).

patterns. This is evident from a comparison with the corresponding experimental diffuse scattering distribution shown in Fig. 6(b). The general shapes of the patterns in Fig. 6(a) and 6(b) are quite similar. Discrepancies in their intensities are mainly due to the different perturbation potentials in the calculation (single-atom potential for the dynamical scattering amplitude) and in the experimentally observed Kikuchi pattern (e.g., atomic vibrations; see also Sec. IV). The correlation between the Kikuchi patterns and the dynamical scattering amplitude should allow us to select regions in reciprocal space where a kinematical interpretation of (azimuthal) reflection profiles is possible.

C. Disordered adsorbate layers

We consider a disordered adsorbate layer where adsorbate atoms (or molecules) are statistically distributed on equivalent sites relative to a perfectly ordered substrate. According to Eq. (14), the diffuse scattering arises from transitions between (2D) Bloch states in the periodic part of the potential where the nonperiodic part is the perturbation. Therefore, one should expect that the diffuse

scattering due to an adsorbate atom is sensitive to its position relative to the substrate. This would offer the possibility to use RHEED as a tool for structure determinations of disordered adsorbate layers, similar to the case of diffuse LEED.³² The results of Sec. II B indicate that the presented approximation works very good if the disorder concerns only the top layer (here the adsorbate layer) of a system.

In order to check whether the diffuse scattering distribution is sufficiently sensitive to the adsorbate position,

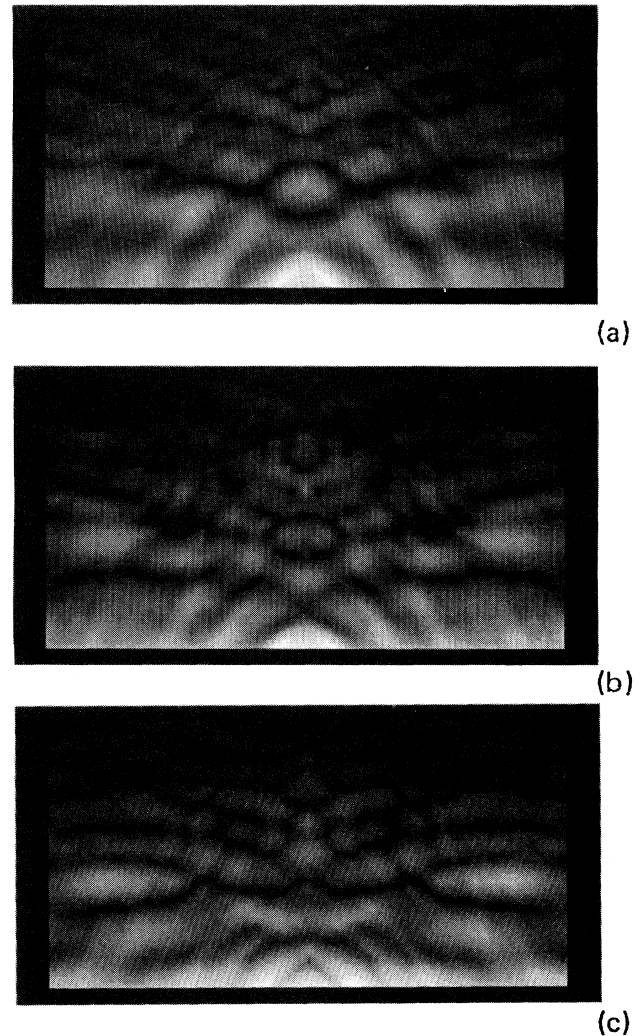


FIG. 7. Calculated diffuse scattering distributions corresponding to three different positions of a model adsorbate atom relative to the substrate [nonreconstructed Pt(110) surface]. Azimuth $[1\bar{1}0]$, 19 keV; 95 mrad, incident glancing angle; angular area, 150×90 mrad, resolution 1×1 mrad. The lower margin corresponds to the polar exit angle 12 mrad; the center of the picture corresponds to the exit azimuth $[1\bar{1}0]$. (a) Adsorbate atom is situated on a hollow site above the topmost layer. The component normal to the surface corresponds to the bulk layer distance 1.386 Å. (b) Same situation as (a) except for an outward relaxation of 0.7 Å. (c) Adsorbate atom "on top" of a substrate atom where the distance between the atomic nuclei is assumed to be 0.7 Å.

corresponding model calculations were performed. For the substrate (periodic-potential part) we chose the non-reconstructed and bulk terminated Pt(110) surface. For simplicity we assumed an adsorbate with a kinematical atomic-scattering factor being proportional to that of Pt. This is justified because only principal effects are of interest here. Furthermore, the reflected amplitude is linear in the perturbation and hence the structure of the diffuse scattering distribution does not depend on the scattering strength of the adsorbate atom.

Figure 7 shows calculated scattering distributions corresponding to three different positions of the adsorbate. All calculations were performed for the same conditions of the incident beam (19 keV, $[1\bar{1}0]$ azimuth, 95 mrad glancing angle). In Figure 7(a) the adsorbate is situated on a hollow site above the topmost substrate layer. The position corresponds to the bulk layer distance of the substrate (1.386 Å). Figure 7(b) shows a similar situation, but an outward relaxation by 0.7 Å was assumed. Both pictures differ significantly. In particular, in the relaxed case the intensity modulation with the polar exit angle is much stronger and faster than in the nonrelaxed case. In Fig. 7(c), the intensity distribution for an adsorbate “on top” of a substrate atom is demonstrated. The distance between the atomic nuclei was assumed to be 0.7 Å. Again, the intensity distribution clearly differs in Figs. 7(a) and 7(b).

These calculations demonstrate that, in principle, diffuse RHEED data are significantly sensitive to adsorbate positions. In the case of real experiments, a problem may arise if other diffuse processes (especially the thermal diffuse scattering) strongly overlap the scattering from the disordered adsorbate layer. To check this, there is a demand for real experiments. It has to be checked under which conditions the data needed for a structural evaluation can be separated from the whole diffuse data.

Alternatively, the thermal diffuse scattering problem in connection with scattering from adsorbates (see above) could be overcome if the broad TDS distribution could be calculated in a comparably simple way, i.e., with a perturbation potential as simple as possible.

IV. THERMAL DIFFUSE SCATTERING

Correlations of thermal vibrations (phonon waves) reveal modulated diffuse Fourier components around the reciprocal lattice points. In the case of not too large electron energies (< 20 keV) these components lead to (dynamically influenced) modulated diffuse intensity contributing partly to the streaks around the sharp reflection spots.^{41–44,33} These contributions depend strongly on the phonon dispersion near the surface and cannot easily be taken into account. However, the possible overlap of TDS and diffuse scattering from the adsorbates concerns rather the overall broad background distribution. The Fourier coefficients due to this part of the TDS are less influenced by the correlations as long as the electron energy is sufficiently low (in the 100-keV energy region diffuse spots corresponding to the three-dimensional bulk structure can appear over the whole observed angular region^{44,45}).

One can therefore speculate whether the broad TDS background can be described in terms of the Einstein model where the vibrational correlations are completely neglected. In order to test that, we have compared corresponding experimental and calculated data.

The classical perturbation potential for thermal vibrations of a single atom is proportional to the gradient of the atomic scattering potential $v(\mathbf{r})$:

$$V_{d,TDS} = \mathbf{d}(t)\nabla v(\mathbf{r}) . \quad (20)$$

$\mathbf{d}(t)$ means the displacement vector at time t . Because the interaction time of the electrons with the surface is small compared with the period of a vibration, the surface can be regarded as “frozen in” and the *intensity* has to be averaged over t . In the case of the Einstein model, the TDS intensity is the incoherent superposition of the scattered intensity of all atoms so that the structure of the scattering distribution depends on $\nabla v(\mathbf{r})$ only.

We have calculated the TDS intensity in this way for the Pt(110)(1×1) surface at $T = 873$ K. The (1×1) structure is due to the (1×2) \rightleftharpoons (1×1) order disorder

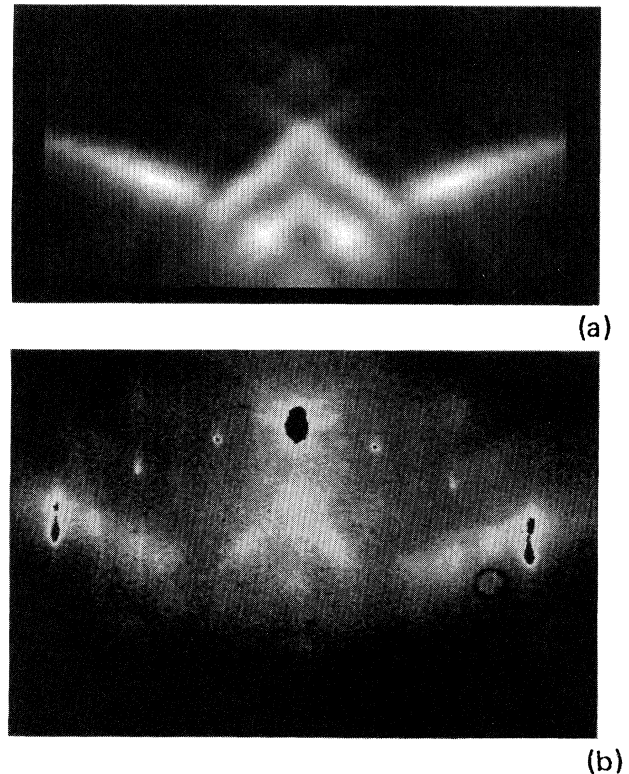


FIG. 8. (a) Calculated thermal diffuse scattering distribution for Pt(110) at 873 K crystal temperature. Independent vibrations of the atoms in the top three layers (Einstein model) have been assumed. Azimuth $[1\bar{1}0]$, 19 keV; incident glancing angle, 95 mrad; angular area, 150×90 mrad; resolution, 1×1 mrad. The lower margin corresponds to the polar exit angle 11 mrad; the center of the picture corresponds to the exit azimuth $[1\bar{1}0]$. (b) Corresponding experimental diffuse scattering distribution. The intensity of the sharp reflections on the Laue circle is artificially reduced.

transition the critical temperature of which was measured as $T_c = 855$ K.¹⁴ Above T_c , one observes sharp integral-order reflections and critical diffuse scattering around the half-order positions. We note that various T_c 's have been reported by different groups.^{46,39,40} Figure 8(a) shows a picture of the calculated TDS intensity ($[1\bar{1}0]$ azimuth, 95 mrad glancing angle, 19 keV). Only the contributions of vibrations along $[001]$ and normal to the surface were taken into account and superimposed incoherently, for the first three layers.

Figure 8(b) illustrates the experimentally diffuse scattering under the same conditions. The intensity of the sharp reflections has been artificially reduced. As the diffuse scattering from the defects in the disordered (1×1) structure is mainly peaked as critical scattering around the half-order positions (not seen under the diffraction conditions where the picture has been recorded), the broad scattering distribution observed should mainly be due to TDS. The agreement between experimental and theoretical scattering distribution is astonishingly good, although a very primitive model for the vibration has been used (no correlations, only three layers). Except for two bright regions at low exit angles in the calculated pattern, the modulations of the diffuse intensity are very well reproduced.

This good agreement again demonstrates that the basic dynamical beam couplings for the diffuse scattering are caused by the periodic part of the whole scattering potential. This beam coupling is obviously mainly responsible for the observed modulations of the broad scattering distribution whereas the correlations between the thermal vibrations seem to play a minor role.

V. CONCLUSION

We have presented a numerically manageable method to compute dynamical diffuse RHEED intensities by perturbation theory where the nonperiodic part of the scattering potential is the perturbation. The dynamical dif-

fuse scattering is assumed as a transition between two-dimensional Bloch states in the periodic part of the potential. The formalism has been tested by means of a simple example.

We have shown that scattering of atoms which are positioned on equivalent sites relative to the periodic potential part can be described as in the kinematical theory, except that the atomic-scattering amplitudes have to be calculated dynamically. These atomic amplitudes f_{dyn} describe the scattering of a single atom being placed in the periodic-potential part of the whole crystal structure.

From a comparison between the modulations of f_{dyn} and the extension of the surface Brillouin zone it follows that azimuthal reflection profiles (parallel to the shadow edge) can often be interpreted kinematically. Polar profiles (normal to the shadow edge) have to be interpreted dynamically.

Model calculations for the diffuse RHEED from a disordered adsorbate layer reveal that the modulations of the corresponding scattering distribution depend strongly on the position of the adsorbate atom relative to the substrate. This possibly allows us to use diffuse RHEED as a method for the structural analysis of disordered adsorbate layers.

The strength of the presented calculational method is further demonstrated for thermal diffuse scattering by means of a comparison with a measured TDS distribution. It turns out that the *broad* scattering distribution is rather influenced by the dynamical scattering within the periodic potential part than by the correlations between the thermal vibrations.

ACKNOWLEDGMENTS

This work was supported by the Stiftung Volkswagenwerk. Furthermore, the authors would like to thank the Höchstleistungsrechenzentrum der KFA, Jülich for the support with computing time on the CRAY-YMP machine. Furthermore, we thank Dr. S. Dudarev for some stimulating discussions.

-
- ¹R. Colella, *Acta Crystallogr. Sec. A* **28**, 11 (1972).
²A. R. Moon, *Z. Naturforsch. A* **27**, 390 (1972).
³P. A. Maksym and J. L. Beeby, *Surf. Sci.* **110**, 423 (1981).
⁴A. Ichimiya, *Jpn. J. Appl. Phys.* **22**, 176 (1983).
⁵T. C. Zhao, H. C. Poon, and S. Y. Tong, *Phys. Rev. B* **38**, 1172 (1988).
⁶G. Meyer-Ehmsen, *Surf. Sci.* **219**, 177 (1989).
⁷S. Nagano, *Phys. Rev. B* **42**, 7363 (1990).
⁸*Electron Diffraction and Reflection Imaging of Surfaces*, edited by P. K. Larsen and P. J. Dobson (Plenum, New York, 1988).
⁹*Kinetics of Ordering and Growth at Surfaces*, edited by M. G. Lagally (Plenum, New York, 1990).
¹⁰N. Chandrasekhar, V. S. Achutharaman, V. Agrawal, and A. M. Goldman, *Phys. Rev. B* **46**, 8565 (1992).
¹¹S. Kohmoto and A. Ichimiya, *Surf. Sci.* **223**, 400 (1989).
¹²M. Stock, J. Risse, U. Korte, and G. Meyer-Ehmsen, *Surf. Sci.* **233**, L243 (1990).
¹³J. M. McCoy, U. Korte, P. A. Maksym, and G. Meyer-Ehmsen, *Surf. Sci.* **261**, 29 (1992).
¹⁴U. Korte and G. Meyer-Ehmsen, *Surf. Sci.* **271**, 616 (1992).
¹⁵C. S. Lent and P. I. Cohen, *Surf. Sci.* **139**, 121 (1984).
¹⁶P. R. Pukite, C. S. Lent, and P. I. Cohen, *Surf. Sci.* **161**, 39 (1985).
¹⁷C. S. Lent and P. I. Cohen, *Phys. Rev. B* **33**, 8329 (1986).
¹⁸X. Tong and P. A. Bennett, *Phys. Rev. Lett.* **67**, 101 (1991).
¹⁹B. A. Joyce, J. H. Neave, P. J. Dobson, and P. K. Larsen, *Phys. Rev. B* **29**, 814 (1984).
²⁰J. L. Beeby, *Reflection High-Energy Electron Diffraction and Reflection Imaging of Surfaces*, edited by P. K. Larsen and P. J. Dobson (Plenum, New York, 1988), p. 29.
²¹G. Meyer-Ehmsen, B. Bölger, and P. K. Larsen, *Surf. Sci.* **224**, 591 (1989).
²²P. K. Larsen, and G. Meyer-Ehmsen, *Surf. Sci.* **240**, 168 (1990).
²³L. M. Peng and J. M. Cowley, *Acta Crystallogr. Sec. A* **42**,

- 545 (1986).
- ²⁴M. G. Knibb, Surf. Sci. **257**, 389 (1991).
- ²⁵D. K. Saldin, J. B. Pendry, M. A. Van Hove, and G. A. Somorjai, Phys. Rev. B **31**, 1985 (1216).
- ²⁶J. Stöhr, R. Jaeger, and S. Brennan, Surf. Sci. **117**, 503 (1983).
- ²⁷S. Kjaer Anderson and A. Howie, Surf. Sci. **50**, 197 (1975).
- ²⁸M. V. Gomoyunova, S. L. Dudarev, and I. I. Pronin, Surf. Sci. **235**, 156 (1990).
- ²⁹J. B. Pendry, Surf. Sci. **57**, 679 (1976).
- ³⁰J. F. L. Hopkinson, J. B. Pendry, and D. J. Titterington, Comput. Phys. Commun. **19**, 69 (1980).
- ³¹U. Korte and G. Meyer-Ehmsen, Surf. Sci. **277**, 109 (1992).
- ³²K. Heinz, D. K. Saldin, and J. B. Pendry, Phys. Rev. Lett. **55**, 2312 (1985).
- ³³S. L. Dudarev, L. M. Peng, and M. I. Ryzanov, Acta Crystallogr. Sec. A **47**, 170 (1991).
- ³⁴H. Niehus, Surf. Sci. **145**, 407 (1984).
- ³⁵G. L. Kellog, Phys. Rev. Lett. **55**, 2168 (1985).
- ³⁶P. Fery, W. Moritz, and D. Wolf, Phys. Rev. B **38**, 7275 (1988).
- ³⁷H. Jagodzinski, W. Moritz, and D. Wolf, Surf. Sci. **77**, 233 (1978).
- ³⁸W. Moritz, H. Jagodzinski and D. Wolf, Surf. Sci. **77**, 249 (1978).
- ³⁹I. K. Robinson, E. Vlieg, and K. Kern, Phys. Rev. Lett. **63**, 2578 (1989).
- ⁴⁰J.-K. Zuo, Y.-L. He, and G.-C. Wang, J. Vac. Sci. Technol. A **8**, 2474 (1990).
- ⁴¹S. Holloway and J. L. Beeby, J. Phys. C **11**, L247 (1978).
- ⁴²B. A. Agrawal, Phys. Rev. B **29**, 814 (1984).
- ⁴³M. Albrecht and G. Meyer-Ehmsen, *Reflection High-Energy Electron Diffraction and Reflection Imaging of Surfaces* (Ref. 20).
- ⁴⁴U. Korte and G. Meyer-Ehmsen, Surf. Sci. **232**, 367 (1990).
- ⁴⁵L. M. Peng and J. M. Cowley, Ultramicroscopy **26**, 227 (1988).
- ⁴⁶K. Dücker and H. P. Bonzel, Europhys. Lett. **7**, 371 (1987).

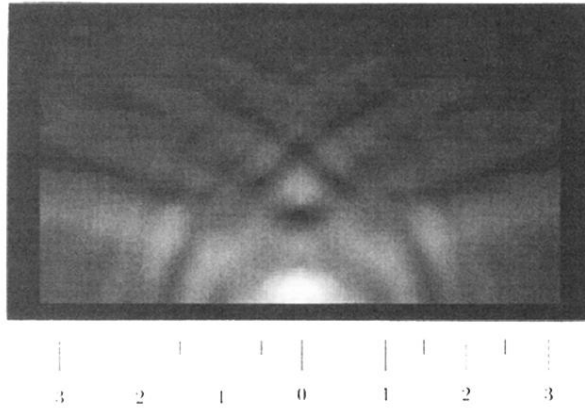


FIG. 4. Calculated scattering distribution from a perturbation atom in the top layer of the Pt(110)(1×2) surface. The atom is situated within the first layer between the atomic rows, i.e., out of phase relative to the (1×2) periodicity. Energy, 19 keV; incident glancing angle, 95 mrad; angular area, 150×90 mrad. The lower margin corresponds to the polar exit angle 12 mrad; the center of the picture corresponds to the exit azimuth $[1\bar{1}0]$. Bright regions mean high intensity. The resolution is 1×1 mrad.

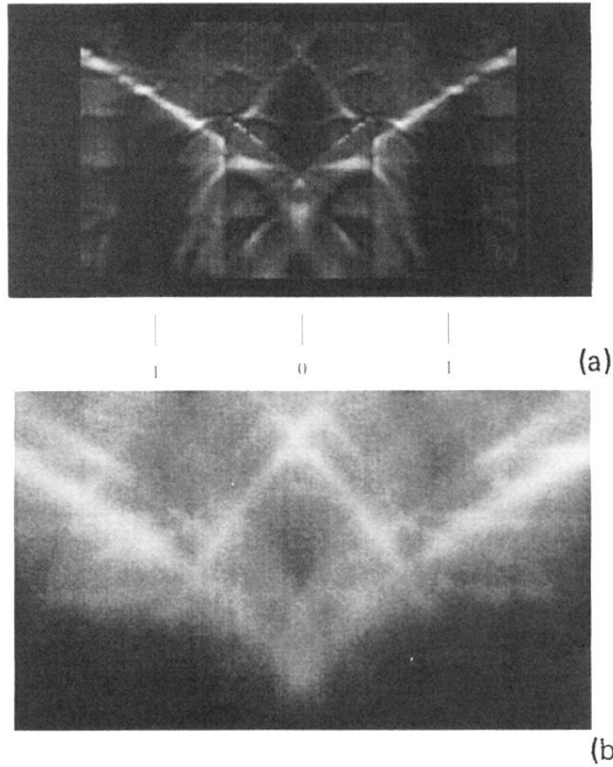


FIG. 6. (a) Calculated scattering distribution from a perturbation atom in the top layer of the Pt(111) surface. The atom is situated on a lattice site. Energy, 19 keV; incident glancing angle, 120 mrad; angular area 190×110 mrad. The lower margin corresponds to the polar exit angle 20 mrad; the center of the picture corresponds to the exit azimuth $[11\bar{2}]$. Bright regions mean high intensity. The resolution is 1×1 mrad. (b) Experimental diffuse scattering distribution for the same angular region. Note the correlation between the Kikuchi patterns in (b) and the features in (a).

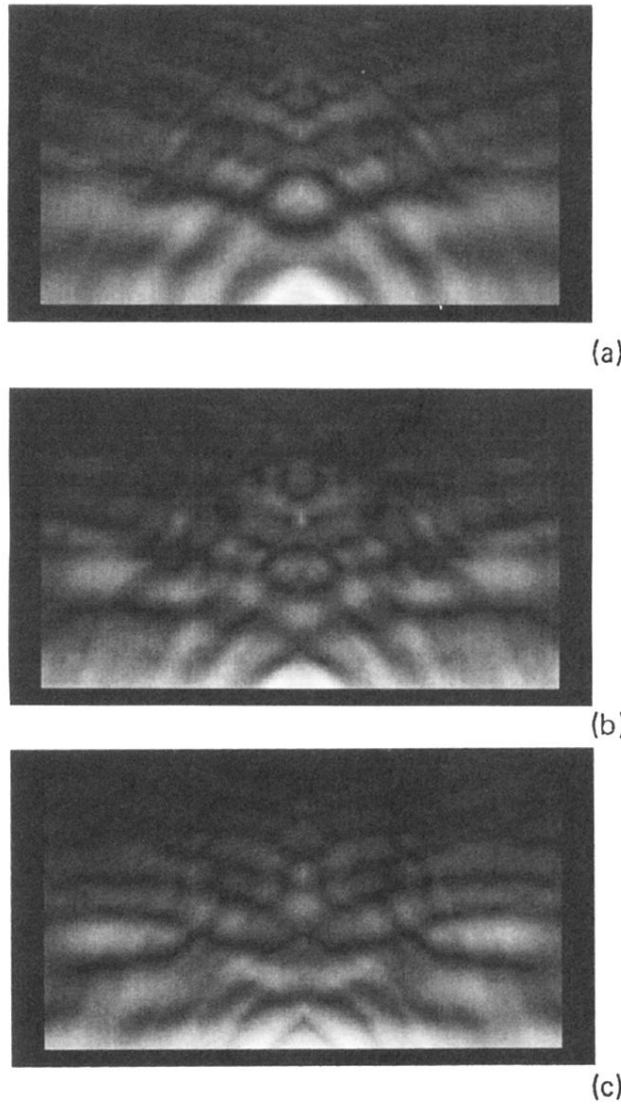


FIG. 7. Calculated diffuse scattering distributions corresponding to three different positions of a model adsorbate atom relative to the substrate [nonreconstructed Pt(110) surface]. Azimuth $[1\bar{1}0]$, 19 keV; 95 mrad, incident glancing angle; angular area, 150×90 mrad, resolution 1×1 mrad. The lower margin corresponds to the polar exit angle 12 mrad; the center of the picture corresponds to the exit azimuth $[1\bar{1}0]$. (a) Adsorbate atom is situated on a hollow site above the topmost layer. The component normal to the surface corresponds to the bulk layer distance 1.386 Å. (b) Same situation as (a) except for an outward relaxation of 0.7 Å. (c) Adsorbate atom "on top" of a substrate atom where the distance between the atomic nuclei is assumed to be 0.7 Å.

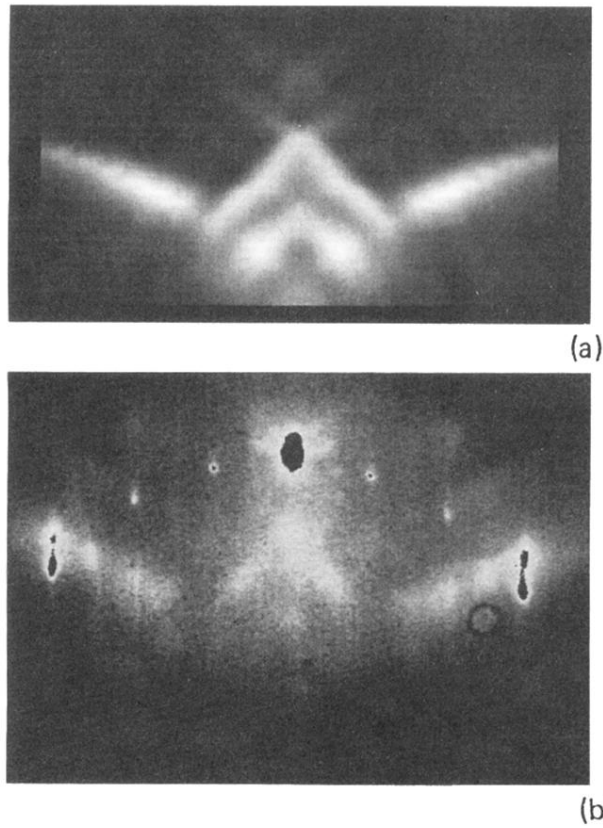


FIG. 8. (a) Calculated thermal diffuse scattering distribution for Pt(110) at 873 K crystal temperature. Independent vibrations of the atoms in the top three layers (Einstein model) have been assumed. Azimuth $[1\bar{1}0]$, 19 keV; incident glancing angle, 95 mrad; angular area, 150×90 mrad; resolution, 1×1 mrad. The lower margin corresponds to the polar exit angle 11 mrad; the center of the picture corresponds to the exit azimuth $[1\bar{1}0]$. (b) Corresponding experimental diffuse scattering distribution. The intensity of the sharp reflections on the Laue circle is artificially reduced.